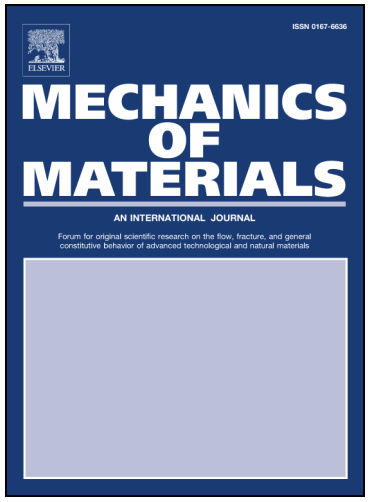

The mechanical reliability of an electronic textile investigated using the virtual-power-based quasicontinuum method

L.A.A. Beex, R.H.J. Peerlings, K. van Os, M.G.D. Geers

PII: S0167-6636(14)00149-5
DOI: http://dx.doi.org/10.1016/j.mechmat.2014.08.001
Reference: MECMAT 2308

To appear in: *Mechanics of Materials*

Received Date: 28 April 2014
Revised Date: 6 August 2014

Please cite this article as: Beex, L.A.A., Peerlings, R.H.J., van Os, K., Geers, M.G.D., The mechanical reliability of an electronic textile investigated using the virtual-power-based quasicontinuum method, *Mechanics of Materials* (2014), doi: http://dx.doi.org/10.1016/j.mechmat.2014.08.001

The mechanical reliability of an electronic textile investigated using the virtual-power-based quasicontinuum method

L.A.A. Beex[a,b,c,*], R.H.J. Peerlings[a], K. van Os[d], M.G.D. Geers[a]

[a] *Department of Mechanical Engineering, Eindhoven University of Technology, P.O. Box 513, 5600 MB Eindhoven, The Netherlands.*
[b] *School of Engineering, Cardiff University, Queen's Buildings, The Parade, Cardiff, CF24 3AA Wales, United Kingdom.*
[c] *Faculté des Sciences, de la Technologie et de la Communication, Université du Luxembourg, 6 rue Richard Coudenhove-Kalergi, L-1359 Luxembourg.*
[d] *Philips Research, High Tech Campus 5, 5656 AE Eindhoven, The Netherlands.*

Abstract

The quasicontinuum (QC) method is a multiscale method for the solution of lattice models that combines coarse-grained regions and fully resolved regions with individual lattice events. QC methodologies are mainly used to reduce the computational costs of conservative atomistic lattice computations. Recently, a virtual-power-based variant has been proposed that enables its use for non-conservative lattice computations. In this contribution the virtual-power-based QC approach is adopted in combination with a recently proposed mesostructural lattice model for electronic textile in order to investigate its mechanical behaviour. The interactions of the lattice model for electronic textile are modelled elasto-plastically and hence, regular conservative QC approaches are not adequate. This article incorporates a modification of a previously defined exact summation rule for QC methods - by sampling the lattice interactions directly instead of via the lattice nodes - which leads to a significant reduction of the computational cost, whereas the accuracy of the summation rule remains unaffected. The presented methodology is used to efficiently investigate the failure envelope of an electronic textile - a woven fabric with embedded electronic components and conduc-

*Corresponding author
Email address: L.A.A.Beex@gmail.com (L.A.A. Beex)

tive wires - and the dependence of the failure envelope on the locations of the conductive wires and the stiffness of the weft yarns is investigated as well.

Keywords: multiscale, quasicontinuum, lattice model, textile, electronic textile, woven, fabric, summation, summation rule

1. Introduction

Electronic textiles are fabrics with embedded electronic components (left in Fig. 1). Conductive wires can be embedded in the fabrics to provide power to the electronic components (right in Fig. 1). One of the future applications of electronic textiles will be in medical applications for the monitoring of functions. Instead of attaching wires and electronic sensors to patients' bodies, they can be embedded in clothing, leading to less discomfort for the patients.

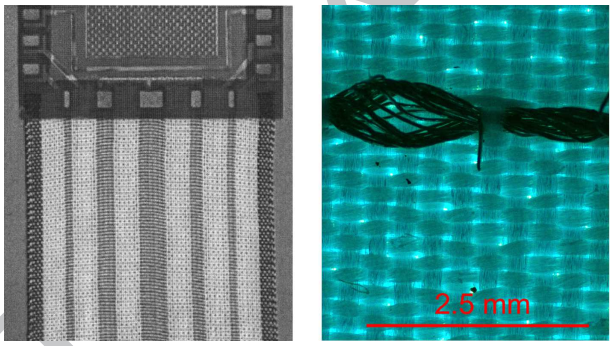

Figure 1: Left: an electronic textile with an electronic component, taken from Marlescu et al. (2003). Right: part of conductive wire (in black) embedded in a woven fabric, taken from Beex et al. (2013a).

In previous studies, it was mainly the electronic functionality of electronic textile that has been investigated (Edmison et al., 2002; Dalton et al., 2003; Marlescu et al., 2003; Bonderover & Wagner, 2004; Coosemans et al., 2006; De Rossi, 2007; Nakad et al., 2007; Zysset et al., 2010). In the study of Bonderover & Wagner (2004) the electrical signal from an inverter woven in a fabric was assessed and the efficiency of cluster computing in an electronic textile was tested by Marlescu et al. (2003). Coosemans et al. (2006) and Zysset et al. (2010) studied the functionality of sensors in electronic textiles for monitoring the human heart and body temperature, respectively.

Mechanical models of electronic textiles can be used to numerically investigate electronic textile's mechanical reliability. Although different models of regular textiles have been proposed (Boisse et al., 2001; Sharma et al., 2003; Sharma & Sutcliffe, 2004; King et al., 2005; Peng & Cao, 2005; Boisse et al., 2006; Lomov & Verpoest, 2006; Zohdi & Powell, 2006; Ben Boubaker et al., 2007a,b; Ten Thije et al., 2007; Lomov et al., 2007; Potluri & Manan, 2007; Potluri & Sagar, 2008; Ten Thije & Akkerman, 2008; Nilakantan et al., 2010), those for electronic textile are scarce. To the best of the authors' knowledge, only in Beex et al. (2013a) the mechanical behavior of an electronic textile was more elaborately considered. A lattice model for an electronic textile with conductive wires woven through the fabric was made and experimentally identified. The interaction with embedded components was not investigated however.

The aim of this work is to investigate the failure envelope of an electronic textile, including an embedded component, using the previously proposed mesostructural lattice model (Beex et al., 2013a) and study how the failure envelope changes if a number of geometrical and material parameters are varied. The electronic textile of interest is a woven fabric with its conductive wires woven through it. Electronic textiles with conductive carbon nanotubes embedded in individual fabric yarns also exist (Dalton et al., 2003; Marlescu et al., 2003), but are not considered here. A computational approach is used in this study, because it allows for an efficient parameter study. Manufacturing a number of different electronic textiles and experimentally testing them is expensive and time consuming. Furthermore, undesired deformation patterns that may occur in experimental testing, e.g. in bias extension testing (Zhu et al., 2007), can be avoided by the selection of appropriate boundary conditions.

The conductive wires must individually be incorporated in the employed mechanical model for the assessment of the mechanical reliability of the considered electronic textile, since (i) the electronic textile becomes useless if one of the conductive wires fails (since one of the electronic components will not have electric power anymore) and (ii) the conductive wires break at significantly smaller strains than the textile yarns. Mesoscale lattice models allow the incorporation of individual yarns and other mesoscopic constituents such as conductive wires (Sharma et al., 2003; Sharma & Sutcliffe, 2004; Beex et al., 2013a). For this reason the mesoscale lattice model used by Beex et al. (2013a) is employed here as well. Its application to electronic textile is illustrated in Fig. 2. An elaborate explanation of the lattice model is given in the next section and of course by Beex et al. (2013a).

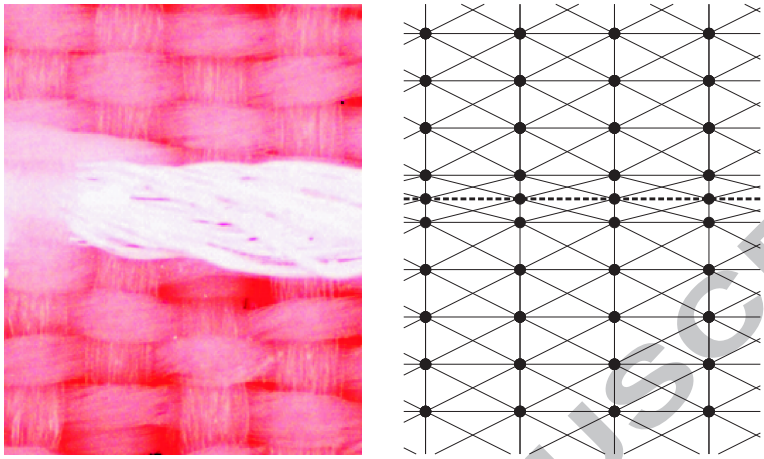

Figure 2: Part of an electronic textile (left, yarns in red, one conductive wire in white) and the lattice model that is used to represent this part (right). The lattice trusses are presented by black lines (solid or dashed) and the lattice nodes are presented as black dots.

Because mesoscale lattice models are computationally expensive for large-scale computations, the principles of the multiscale quasicontinuum (QC) method (Tadmor et al., 1996a) are used in this study to reduce the computational costs of the large-scale computations required for electronic textile. Conservative QC methodologies have been used to study the atomistic mechanics of metals (Tadmor et al., 1996a,b; Knap & Ortiz, 2001; Miller & Tadmor, 2002; Marian et al., 2008; Eidel & Stukowski, 2009) and even the mechanical behaviour of the walls of red blood cells (Wang et al., 2014). Recently, they have been formulated in a thermodynamical setting that extends their use for non-conservative lattices (Beex et al., 2014b,a), as required for electronic textile.

Similar to the multiscale approach of Nilakantan et al. (2010), QC approaches combine fine-scale regions containing small-scale mechanisms with coarse-scale domains in which computational savings are made. A QC approach presents two advantages compared to concurrent multiscale approaches such as the one of Nilakantan et al. (2010). These advantages originate from the use of the lattice model in the entire modeling domain, i.e.:

- no internal interfaces occur between coarse domains and regions of interest and hence, no coupling procedures are required. Note that

this only holds for entirely nonlocal QC approaches (Knap & Ortiz, 2001; Eidel & Stukowski, 2009; Beex et al., 2011, 2013c).

- No associated continuum description is required in the coarse domain. This can be considered as an advantage, since large yarn rotations are not automatically incorporated in continuum descriptions (Peng & Cao, 2005; Ten Thije et al., 2007; Ten Thije & Akkerman, 2008), but they are naturally included in lattice models (Sharma et al., 2003; Sharma & Sutcliffe, 2004; Beex et al., 2013a).

A disadvantage of the employed QC approach is that detailed microscale mechanisms, as incorporated by Nilakantan et al. (2010), are not directly taken into account in this approach. They can be accounted for in an indirect manner only; by lumping them in the material descriptions of the lattice models' elements.

QC approaches use two principles to reduce the computational costs of direct lattice computations. First, interpolation is applied to reduce the degrees of freedom of the lattice model. Second, the selection of only a small number of lattice nodes is used to approximate the governing equations. The way these lattice nodes are selected are defined in summation rules. Because QC methods originate from atomistic computations, the selection is based on lattice nodes (atoms when applied to atomistic computations). However, for structural lattices no need exists to select lattice interactions via the lattice nodes, but the interactions can be selected directly. In this paper, the influence of interaction-based summation is investigated for the summation rule proposed by Beex et al. (2011), which determines the governing equations exactly instead of approximating them.

Hence, the novelties of this paper are that:

- the virtual-power-based QC method is used to investigate the mechanical behaviour of a true material,
- the influence of geometric and material parameters on the mechanical reliability of an electronic textile with an embedded component is investigated, and
- interaction-based summation, in contrast to node-based summation, is used to reduce the efforts to construct the governing equations.

A detailed description of the adopted lattice model and the virtual-power-based QC methodology is given, in order to make the paper self-contained. The outline is as follows. First, the formulation of the lattice model for electronic textile and its experimental identification procedure are discussed. Subsequently, the principles of the virtual-power-based QC method related to the lattice model for electronic textile are detailed and the aforementioned modification of the exact summation rule (Beex et al., 2011) is explained. In the subsequent section, the virtual-power-based QC framework including the mesoscopic lattice model for electronic textile is used for a parameter study of a patch of electronic textile with one embedded rectangular electronic component. Patches of electronic textile with this component are subjected to several macroscale deformation modes. The macroscale strains at which the conductive wires fail are determined, resulting in macroscale failure surfaces. Finally, conclusions are presented.

2. Lattice model for electronic textile

In this section, the lattice model for electronic textile is discussed. The electronic textile and the lattice model are shown in Fig. 2. The electronic textile is a woven fabric with conductive wires woven through it. The warp direction is the horizontal direction in Fig. 2, whereas the vertical direction corresponds to the so-called weft direction.

The lattice model consists of lattice trusses (i.e. springs) connected to each other at lattice nodes. The horizontal and vertical lattice trusses represent yarn segments. The diagonal trusses describe the shear response (Sharma et al., 2003; Sharma & Sutcliffe, 2004; Beex et al., 2013a) which is physically governed by friction in the yarn-to-yarn contact areas if rotation occurs between the warp and weft yarns or/and between the conductive wires and weft yarns.

The lattice nodes are only present at the locations where warp yarn segments, weft yarn segments and conductive wire segments are in contact. Since the lattice trusses are pin-jointed in these lattice nodes, it is assumed that yarn segments and conductive wire segments cannot slide with respect to each other, although this can be included in lattice models as well (Ridruejo et al., 2010; Kulachenko & Uesaka, 2012; Wilbrink et al., 2013).

In addition to the lattice model proposed by Beex et al. (2013a), the conductive wire segments are individually incorporated by using their respective material response in the lattice trusses that represent them (shown as dashed

lines in Fig. 2). The cross-sectional area of the conductive wires in the actual electronic textile on the left in Fig. 2 is large compared to that of the yarns. As a result, the yarns near conductive wires are compressed together, which is difficult to incorporate in a lattice model. To overcome this in the lattice, it is chosen to give the conductive wires a significantly smaller cross-sectional area than those on the left in Fig. 2, so that the lattice model as presented on the right in Fig. 2 is valid.

The diagonal lattice trusses connected to the lattice trusses representing conductive wire segments are given the same material description as the other diagonal lattice trusses. This means that the rotational response, that comes into play when conductive wire segments rotate relative to weft yarn segments, is assumed to be almost the same as that between warp and weft yarn segments (note that the length of the diagonal trusses connected to lattice trusses representing conductive wire segments is smaller, resulting in a slightly different local response).

2.1. Thermodynamical setting of the lattice model

The descriptions of the lattice trusses are required to be non-linear as the experimentally recorded responses in the right image of Fig. 3 indicate. In this study, this is accomplished by using an elasto-plastic model for the lattice trusses, as done by Beex et al. (2013a). Hence, dissipation occurs in the lattice model and to accurately account for this, the thermodynamical setting for the lattice model with dissipation in the trusses is derived first. This thermodynamical setting also forms the basis for the virtual-power-based quasicontinuum formulation of the lattice model (Germain, 1973; Beex et al., 2014b,a).

Consider a lattice model containing t lattice trusses and n lattice nodes. The lattice truss numbers are stored in index set $T = \{1, .., t\}$ and the lattice node numbers in index set $N = \{1, .., n\}$. The displacement components of the lattice nodes are stored in column matrix $\mathbf{u}$, which is for a two-dimensional lattice of size $2n \times 1$. Furthermore, since the lattice includes dissipation, internal history variables related to dissipation are defined; they are stored in column matrix $\mathbf{z}$. For the considered lattice with elastoplastic trusses, the size of $\mathbf{z}$ is $t \times 1$, since each of the t lattice trusses contains one dissipation mechanism.

For the considered lattice, the internal power associated with a virtual velocity $\dot{\mathbf{u}}$ should equal the power provided to the lattice. This is expressed as follows:

$$\dot{\mathbf{u}}^T\mathbf{F} = \dot{\mathbf{u}}^T\mathbf{G} \qquad \forall\dot{\mathbf{u}}, \tag{1}$$

where $\mathbf{F}$ is the column matrix containing the components of the internal forces and $\mathbf{G}$ is the column matrix containing the components of the externally applied forces. Both column matrices are of length $2n$.

The internal power is the sum of the rate of the energy stored in the lattice, $\dot{E}$, and the rate of dissipation occurring in the lattice, $\dot{D}$:

$$^{int}P = \dot{E} + \dot{D}. \tag{2}$$

An expression for the rate of the energy stored in the lattice can be derived using the chain rule, since the stored energy depends on the kinematic and internal history variables, i.e. $E = E(\mathbf{u}, \mathbf{z})$. The time-derivative of the stored energy thus reads:

$$\dot{E} = \dot{\mathbf{u}}^T\frac{\partial E}{\partial \mathbf{u}} + \dot{\mathbf{z}}^T\frac{\partial E}{\partial \mathbf{z}}. \tag{3}$$

By substitution of Eq. (3) and Eq. (1) in Eq. (2), the following expression is obtained for the rate of the dissipation:

$$\dot{D} = \dot{\mathbf{u}}^T\left(\mathbf{F} - \frac{\partial E}{\partial \mathbf{u}}\right) - \dot{\mathbf{z}}^T\frac{\partial E}{\partial \mathbf{z}}. \tag{4}$$

Now it is assumed that if the internal history variables remain constant ($\dot{\mathbf{z}} = \mathbf{0}$), no dissipation occurs in the lattice ($\dot{D} = 0$). This should hold for any $\dot{\mathbf{u}}$ leading to the classical expression for the internal forces $\mathbf{F}$:

$$\mathbf{F} = \frac{\partial E}{\partial \mathbf{u}}. \tag{5}$$

The rate of dissipation, which should be non-negative, now reads:

$$\dot{D} = -\dot{\mathbf{z}}^T\frac{\partial E}{\partial \mathbf{z}} \geq 0, \tag{6}$$

or:

$$\dot{D} = \dot{\mathbf{z}}^T \mathbf{F}_z \geq 0 \qquad \text{with} \qquad \mathbf{F}_z = -\frac{\partial E}{\partial \mathbf{z}}. \tag{7}$$

$\mathbf{F}_z$ is the column matrix of the dissipation forces.

Explicit expressions for the stored energy E and the dissipation potential, Φ, now need to be specified. The latter must be defined such that it satisfies the condition in (7). For the considered lattice with t elastoplastic trusses, the stored energy and dissipation potential can be constructed as the corresponding sum of the individual trusses:

$$E = \sum_{i=1}^{t} E_i \tag{8}$$

$$\Phi = \sum_{i=1}^{t} \Phi_i. \tag{9}$$

Note that for QC methodologies, it is standard to sum first over the lattice nodes and then over the half of the stored energies and dissipation potentials (compare e.g. Eq. (8) to Eq. (30)).

Next, the stored energy and dissipation potential for an individual truss needs to be expressed so that the lattice model captures the mechanical response of the electronic textile accurately. Both expressions are derived below, based on the experimentally recorded responses of the electronic textile and individual conductive wires.

2.2. Experimental identification

It may be complex to experimentally identify lattice models, since all lattice interactions are interconnected. Lattice models using trusses for textile materials however, can be experimentally identified in a straightforward manner, as shown by Beex et al. (2013a). The stored energy and dissipation potential of the three types of lattice springs in a unit cell (see the left image Fig. 3) can directly be identified from the tensile responses in the same direction as the orientation of each of these lattice trusses.

For the three types of lattice trusses that represent the fabric, the measured responses on patches of electronic textile first need to be converted to the responses of the individual lattice trusses. For this, the ratios between the cross-sectional area of the yarns and the area that is spanned by the yarns in the fabric, need to be incorporated. This is explained in more detail in Beex et al. (2013a). The responses resulting from this conversion are shown on the right in Fig. 3.

Subsequently, the mechanical behaviour of a unit cell of the lattice model (left in Fig. 3) needs to be considered. If a unit cell is loaded in tension in warp direction (the horizontal direction in Fig. 3), only the horizontal lattice trusses (blue in Fig. 3) contribute to the tensile response, because the diagonal lattice trusses (magenta, the left image of Fig. 3) have a significantly more compliant tensile response than the horizontal lattice trusses. This can be verified by comparing the warp response (blue, right image of Fig. 3) to the diagonal response (magenta, right image of Fig. 3). Hence, the diagonal trusses do not contribute to the warp response of a unit cell. As a result, the experimentally recorded tensile response of the fabric in warp direction can be directly employed to identify the tensile material description of the horizontal lattice trusses.

This assumption is also valid for the weft direction because the experimental response in weft direction (the red curve in the right image of Fig. 3) is also significantly stiffer than the diagonal response (the magenta curve in the right image of Fig. 3). Hence, the measured weft response can also directly be used to identify the tensile material description of the vertical lattice trusses representing the weft response.

The compressive responses of all lattice trusses are taken significantly more compliant than the tensile responses, because in compression it is assumed that the yarns buckle.

This insignificant compressive response also has the advantage that the tensile material description of the diagonal lattice trusses can be identified from the in-plane tensile response measured in the direction of the diagonal trusses (bias extension testing). If the unit cell (left in Fig. 3) is loaded in diagonal direction, the diagonal lattice truss that is oriented in the loading direction elongates, whilst the other diagonal lattice truss is compressed. Since this compression occurs with a negligible force, the remaining four lattice trusses that represent warp and weft yarn segments act as a mechanism and also do not contribute to the observed response.

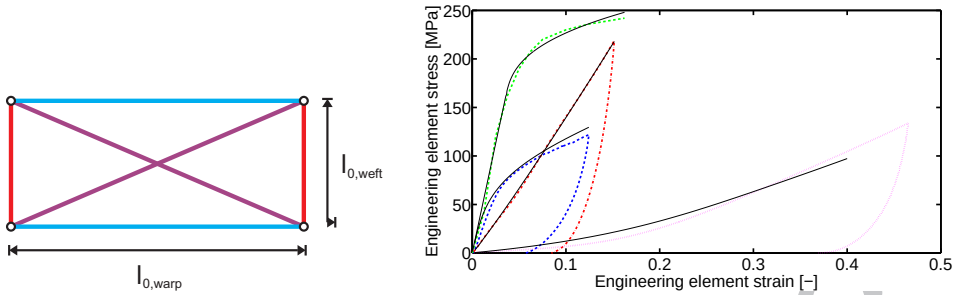

Figure 3: A unit cell of the lattice model on the left and on the right the response of the electronic textile in warp (blue), weft (red) and diagonal (purple) direction, as well as the response of an individual conductive wire (green). The responses of a unit cell of the textile and the response of an individual truss representing the conductive wire segments are shown in black.

2.3. Expressions for the stored energy and dissipation potential of the lattice trusses

Accurate expressions for the stored energy and dissipation potential of the individual lattice trusses are now required, i.e. expressions for E_i and Φ_i. For all lattice trusses, it is chosen to use a linear elastic description coupled with non-linear hardening plasticity. As mentioned before, the compressive responses are very compliant and are modelled fully elastically.

Using an additive split into elastic and plastic parts of the total strain and defining the total strain as a linear function of the elongation (Beex et al., 2014b), the following expression for the stored energy in an elastoplastic truss i, E_i in Eq. (8), is adopted:

$$E_i = \begin{cases} \frac{1}{2} A_i L_i Y_i^{ten} \left(\frac{\Delta L_i}{L_i} - z_i \right)^2 & \text{if} \quad \frac{\Delta L_i}{L_i} - z_i \geq 0 \\ \frac{1}{2} A_i L_i Y_i^{com} \left(\frac{\Delta L_i}{L_i} - z_i \right)^2 & \text{if} \quad \frac{\Delta L_i}{L_i} - z_i < 0, \end{cases} \tag{10}$$

where

$$\Delta L_i = |\vec{x}_l + \vec{u}_l - \vec{x}_k - \vec{u}_k| - |\vec{x}_l - \vec{x}_k|, \tag{11}$$

$$L_i = |\vec{x}_l - \vec{x}_k|, \tag{12}$$

where the constants A_i, Y_i^{ten} and Y_i^{com} are the original cross-sectional area, the Young's modulus in tension and the Young's modulus in compression of truss i, respectively. The original length of truss i and the total change in length of truss i are represented by L_i and ΔL_i, respectively. The original location vectors and displacement vector of the two lattice nodes connected to truss i are given by $\vec{x}$ and $\vec{u}$, respectively, where the subscripts refer to one of the two nodes ($k, l \in N$). The internal variable z_i, the ith component of the column matrix with internal history variables $\mathbf{z}$, corresponds to the plastic strain of truss i.

The highly non-linear parts of the tensile responses in Fig. 3 are captured by a power-law hardening. This is expressed as follows by the dissipation potential of truss i (Φ_i in Eq. (9)):

$$\Phi_i = (F_z)_i - A_i L_i \sigma_i^{y0} \left(1 + H_i (\alpha_i)^{m_i} \right), \tag{13}$$

where σ_i^{y0} is the initial yield stress of truss i and H_i and m_i are hardening parameters of truss i and $(F_z)_i = -\frac{\partial E}{\partial z_i} = -\frac{\partial E_i}{\partial z_i}$ (according to Eq. (7)). Furthermore, α_i is an internal history variable that defined by:

$$\dot{z}_i = \dot{\alpha}_i \frac{\partial \Phi}{\partial (F_z)_i} = \dot{\alpha}_i \frac{\partial \Phi_i}{\partial (F_z)_i} = \dot{\alpha}_i, \tag{14}$$

which makes α_i the effective plastic strain (or equivalent plastic strain) of truss i. Hence, for the considered lattice model the effective plastic strain equals the plastic strain ($\boldsymbol{\alpha} = \mathbf{z}$), because plastic deformation is only allowed to occur in tension (see Eq. (13)).

To ensure that the rate of dissipation of a single truss is never smaller than zero, the following Kuhn-Tucker conditions apply:

$$\dot{\alpha}_i \geq 0 \qquad \Phi_i \leq 0 \qquad \dot{\alpha}_i \Phi_i = 0. \tag{15}$$

Note that this also ensures that the total rate of dissipation in Eq. (6) is non-negative.

The expressions for the stored energy in Eq. (10) and dissipation potential in Eq. (13) are also used for the lattice trusses representing the conductive wire segments. The material responses for the conductive wire segments have been characterized experimentally by carefully removing the textile yarns from the conductive wires (so that no plastic deformation occurred during this process) allowing to test the conductive wires individually. The influence of wire-to-yarn compression of the conductive wires in wire-to-yarn contact points is therefore not taken into account. All geometric and material parameters used in the expressions of the stored energy and the dissipation potential for the three types of lattice trusses representing the fabric and the type of lattice truss representing the conductive wires are given in Table 1.

Table 1: Geometric and material parameters of the four types of trusses. The four types are distinguished by their physical meaning.

	Warp yarn segment	Weft yarn segment	Rotational stiffness	Cond. wire segment
A [μm^2]	15.5e3	15.5e3	15.5e3	1.26e3
L [μm]	288	161	330	288
Y^{ten} [GPa]	4.141	7.723	4.334	4.512
Y^{com} [GPa]	0.01	0.01	0.01	0.01
σ^{y0} [MPa]	0.2	0.2	0.2	172
H [MPa]	238	2.12e3	815	196
m [-]	0.289	1.089	2.088	0.369

The responses of the lattice trusses are shown in Fig. 3. They correspond accurately with the responses of the electronic textile and an individual conductive wire. Note that the three presented responses of the unit cell (not the response of the lattice truss representing a conductive wire segment) include the influence of the remaining trusses in a unit cell. These responses are not the identified single trusses, but still correspond accurately with the observed behaviour. This indicates that the direct identification procedure is valid. Note also that the diagonal response of the unit cell only reaches approximately 40% engineering strain, because at this strain the unit cell collapses.

2.4. Solving the governing equations

The governing equations of the lattice model are the virtual-power statement in Eq. (1) (which must hold for all virtual velocities $\dot{\mathbf{u}}$), and the Kuhn-Tucker conditions in Eq. (15) (which must hold for all t lattice trusses). Using a first-order Taylor-expansion, a Newton-Raphson solution procedure can be used to solve them. A modified Newton-Raphson procedure is required - in contrast to a standard Newton-Raphson procedure. The reason for this is that the hardening of the diagonal trusses is so gradual, that in our implementation (in MATLAB) the corrections to the kinematic variables become infinitely larger. The modified Newton-Raphson procedure for the lattice can be expressed as follows:

$$\dot{\mathbf{u}}^T \Big(\mathbf{F}(\mathbf{u}^*, \mathbf{z}^*) + \mathbf{K}(\mathbf{u}^0, \mathbf{z}^0) d\mathbf{u} \Big) = \dot{\mathbf{u}}^T \mathbf{G} \qquad \forall \dot{\mathbf{u}}, \tag{16}$$

where $\mathbf{u}^*$ and $\mathbf{z}^*$ are the kinematic and internal history variables computed in the previous iteration, $\mathbf{u}^0$ and $\mathbf{z}^0$ are the initial kinematic and internal history variables (i.e. $\mathbf{u}^0 = \mathbf{0}$ and $\mathbf{z}^0 = \mathbf{0}$), and $d\mathbf{u}$ are the corrections to the kinematic variables computed in the current iteration. The corrected values of the internal history variables are found by satisfying the Kuhn-Tucker relations in Eq. (15) for each lattice truss in the current iteration. In Eq. (16), $\mathbf{K}$ is the stiffness matrix. The internal force column matrix and the stiffness matrix are determined as follows:

$$\mathbf{F} = \frac{\partial E}{\partial \mathbf{u}} = \sum_{i=1}^{t} \frac{\partial E_i}{\partial \mathbf{u}} \tag{17}$$

$$\mathbf{K} = \frac{\partial}{\partial \mathbf{u}} \left(\frac{\partial E}{\partial \mathbf{u}} \right) = \sum_{i=1}^{t} \frac{\partial}{\partial \mathbf{u}} \left(\frac{\partial E_i}{\partial \mathbf{u}} \right), \tag{18}$$

respectively, and their scalar components are given by:

$$(F)_p = \sum_{i=1}^{t} \frac{\partial E_i}{\partial u_p}, \tag{19}$$

$$(K)_{pq} = \sum_{i=1}^{t} \frac{\partial}{\partial u_q}\left(\frac{\partial E_i}{\partial u_p}\right), \tag{20}$$

respectively, where p and q run over all components of $\mathbf{u}$.

The limitation of the system given by Eq. (16) and Eq. (15) is the computational overload for practically relevant electronic textile designs, since many lattice nodes and lattice trusses are required. The large number of n lattice nodes means that the system of $2n$ scalar equations resulting from Eq. (16) is computationally expensive. Furthermore, the large number of t lattice trusses leads to substantial efforts in the construction of the force column $\mathbf{F}$ and the stiffness matrix $\mathbf{K}$ and the procedure enforceing the Kuhn-Tucker conditions in Eq. (15).

3. Virtual-power-based QC method

To reduce the computational costs of large-scale lattice computations, the quasicontinuum (QC) method (Tadmor et al., 1996a) will be used, which introduces two remedies to overcome the significant computational costs of large-scale lattice computations. The two remedies are (i) interpolation to reduce the number of degrees of freedom (DOFs) and (ii) summation to reduce the efforts to construct the governing equations. In Fig. 4 the two remedies are illustrated as two subsequent reduction steps. In each reduction step an error, e, may be introduced. It is necessary to keep the total error, e_{tot}, that occurs between the direct lattice computation and the QC computation small, still reducing the computational cost of the simulation significantly.

3.1. Interpolation

The use of interpolation ensures a significantly smaller number of DOFs, making the interpolated (i.e. condensed) alternative of Eq. (16) significantly more efficient to solve. Interpolation is used to express the displacement components of all n lattice nodes as a function of the displacement components of only a small number of r lattice nodes. These r lattice nodes are often referred to as representative nodes or repnodes (or repatoms if the QC method is applied to atomistic lattices). The r repnodes, stored in subset R, are selected from all lattice nodes ($R \subseteq N$).

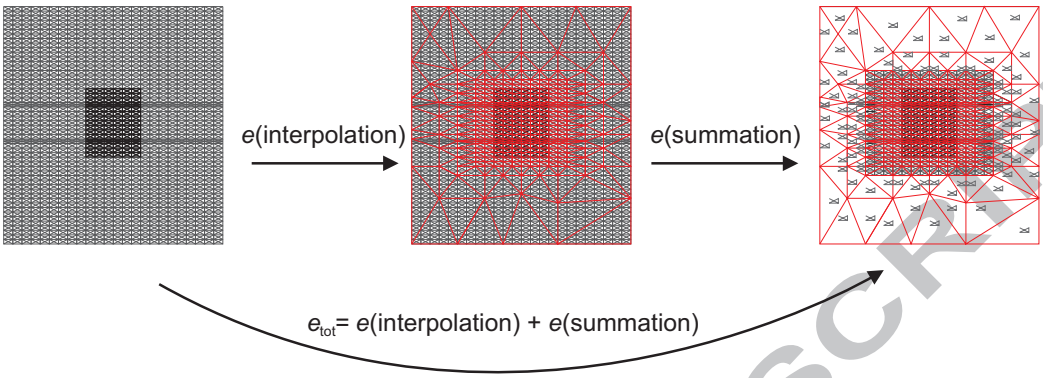

Figure 4: Schematic illustration of the two reduction steps introduced in the QC method (i.e. interpolation and summation) applied to the lattice model for electronic textile. The lattice model is shown in grey and the lattice trusses that correspond to a stiff component are shown in black. Interpolation triangles are shown in red. During both reduction steps an error e may be introduced.

In QC approaches, linear interpolation triangles are mainly used to interpolate the displacement components of the lattice nodes between the repnodes. Hence, the interpolation functions of the triangles in Fig. 4 are identical to the shape functions used for linear triangular finite elements (FEs). As a result of this similarity, developments made in FE technologies, e.g. adaptive remeshing, can also be used in QC methodologies (Shenoy et al., 1999).

The use of these interpolation triangles leads to a true multiscale approach. Consider for instance the centre image in Fig. 4 in which a stiff region is introduced by modelling the lattice trusses in a rectangular domain significantly stiffer than those in the remaining domain. For the application to electronic textile, this stiff region represents an electronic component. If this model is e.g. uniformally deformed, affine deformations will occur everywhere except around the electronic component. In order to capture these fluctuations, all lattice nodes are selected as repnodes in this region. As a result, the mesoscale lattice model is fully resolved here, whereas in the remaining part of the domain the lattice is interpolated, where only the effective macroscale properties of the lattice model are captured.

The error due to interpolation (e(interpolation) in Fig. 4) remains small if large interpolation triangles are only used in regions with small displacement fluctuations. The following approximation for the displacement components of all lattice nodes then holds:

$$\mathbf{u} \approx \bar{\mathbf{u}} = \mathbf{\Psi}\mathbf{u}_r, \tag{21}$$

where $\mathbf{u}_r$ represents the column of length $2r$ that includes the displacement components of the r repnodes. The matrix containing the interpolation function evaluations at the locations of all n lattice nodes is represented by $\mathbf{\Psi}$ which is of size $2n \times 2r$. If $\mathbf{u} \approx \bar{\mathbf{u}}$, the stored energy of the condensed system hardly differs from that of the full system, nor will be the dissipation of the condensed system, i.e. $E \approx \bar{E}$ and $\Phi \approx \bar{\Phi}$.

As a result of substituting Eq. (21) in Eq. (16) the linearized virtual-power statement of the condensed lattice reads:

$$\dot{\mathbf{u}}_r^T \left(\mathbf{\Psi}^T \mathbf{F}(\bar{\mathbf{u}}^*, \mathbf{z}^*) + \mathbf{\Psi}^T \mathbf{K}(\bar{\mathbf{u}}^*, \mathbf{z}^*) \mathbf{\Psi} d\mathbf{u} \right) = \dot{\mathbf{u}}_r^T \mathbf{\Psi}^T \mathbf{G} \qquad \forall \dot{\mathbf{u}}_r, \tag{22}$$

where a condensed force column, $\bar{\mathbf{F}}$, and a condensed stiffness matrix, $\bar{\mathbf{K}}$, can be identified as $\mathbf{\Psi}^T\mathbf{F}$ and $\mathbf{\Psi}^T\mathbf{K}\mathbf{\Psi}$, respectively. They can be determined as follows:

$$\bar{\mathbf{F}} = \mathbf{\Psi}^T \sum_{i=1}^{t} \frac{\partial E_i}{\partial \mathbf{u}} \tag{23}$$

$$\bar{\mathbf{K}} = \mathbf{\Psi}^T \sum_{i=1}^{t} \frac{\partial}{\partial \mathbf{u}} \left(\frac{\partial E_i}{\partial \mathbf{u}} \right) \mathbf{\Psi}. \tag{24}$$

Eq. (22) results in a system of $2r$ scalar equations and is thus significantly more efficient to solve than the original system of $2n$ scalar equations (provided that $r \ll n$). However, still all t lattice trusses must be visited to construct $\bar{\mathbf{F}}$ and $\bar{\mathbf{K}}$ and all t lattice nodes must satisfy the t Kuhn-Tucker conditions in Eq. (15). Hence, the procedure to construct the governing equations remains computationally inefficient at this point.

Note that the linearized virtual-power balance in Eq. (22) results from substitution of Eq. (21) in Eq. (16). If one derives the thermodynamical setting from the beginning for the interpolated lattice model, Eq. (22) also results. Hence, the virtual-power-based QC framework is energetically consistent.

3.2. Summation

The second reduction step introduced in the QC method is to approximate the condensed stored energy and condensed dissipation by visiting a small number of s lattice trusses, instead of determining them by visiting all t lattice nodes. This procedure is substantially more efficient if $s \ll t$. The small number of s lattice trusses (stored in S, where $S \subseteq T$) are used to sample those in their vicinity. Therefore, we will refer to them as sampling trusses. The number of lattice trusses that each sampling truss i represents is summed in the corresponding weight factor, w_i (including the sampling truss i itself). The stored energy thus reads:

$$E \approx \bar{E} \approx \tilde{\bar{E}} = \sum_{i \in S} w_i \bar{E}_i, \tag{25}$$

where $\tilde{\bar{E}}$ is the stored energy of the interpolated, summed lattice.

To ensure that the dissipation is consistent with the summation, the dissipation potential of sampling truss i is expressed as follows:

$$\tilde{\bar{\Phi}}_i = (\tilde{\bar{F}}_z)_i - w_i A_i L_i \sigma_i^{y0} \left(1 + H_i (\alpha_i)^{m_i} \right) \tag{26}$$

$$= w_i (\bar{F}_z)_i - w_i A_i L_i \sigma_i^{y0} \left(1 + H_i (\alpha_i)^{m_i} \right), \tag{27}$$

where $\tilde{\bar{\Phi}}_i$ is the dissipation potential of sampling truss i in the interpolated, summed system. Substitution of Eq. (25) in Eq. (23) and Eq. (24) now leads to the following expressions for the condensed, summed force column, $\tilde{\bar{\mathbf{F}}}$, and the condensed, summed stiffness matrix, $\tilde{\bar{\mathbf{K}}}$:

$$\tilde{\bar{\mathbf{F}}} = \mathbf{\Psi}^T \sum_{i \in S} w_i \frac{\partial E_i}{\partial \mathbf{u}} \tag{28}$$

$$\tilde{\bar{\mathbf{K}}} = \mathbf{\Psi}^T \sum_{i \in S} w_i \frac{\partial}{\partial \mathbf{u}} \left(\frac{\partial E_i}{\partial \mathbf{u}} \right) \mathbf{\Psi}. \tag{29}$$

Note that the expressions for the force column and stiffness matrix are in agreement with energy-based summation rules (Eidel & Stukowski, 2009; Beex et al., 2011, 2013c), since p and q run over all components of $\mathbf{u}$.

3.3. Interaction-based summation

The question at this point is which lattice trusses must be selected such that $\bar{E} \approx \tilde{\bar{E}}$ and $\bar{\Phi} \approx \tilde{\bar{\Phi}}$ (and hence, $\bar{\mathbf{F}} \approx \tilde{\bar{\mathbf{F}}}$ and $\bar{\mathbf{K}} \approx \tilde{\bar{\mathbf{K}}}$), i.e. which lattice trusses must be selected such that the error due to summation is small (see Fig. 4). The selection of the sampling trusses, including the computation of w_i and the manner in which the sampling trusses are treated (locally or non-locally) are generally referred to as a summation rule. Several summation rules can be found in literature, such as those proposed in studies of Tadmor et al. (1996a,b); Knap & Ortiz (2001); Miller & Tadmor (2002); Eidel & Stukowski (2009); Beex et al. (2011) and Beex et al. (2013c).

In this study, the summation rule of Beex et al. (2011) is used, which has the advantage that no error due to summation occurs (i.e. the second step in Fig. 4 is exact). The only approximation made is therefore in the interpolation and it results in highly accurate QC computations if adequate interpolation triangulations are used. The exact summation of Beex et al. (2011) is based on the fact that for linear interpolation, all the same types of lattice interactions (for the considered X-braced lattice model four types can be distinguished), which are entirely located within one interpolation triangle, have the same stored energy. Hence, we can only select one of each type in each interpolation triangle and account for the others through the weight factor. All the lattice interactions that cross a triangle edge, may have a potentially unique stored energy and are taken discretely into account (with $w_i = 1$).

However, the summation rule of Beex et al. (2011) is expressed in terms of sampling points, as it originates from atomistic computations in which the total stored energy is expressed in terms of site-energies. If we apply it to the lattice considered here, the following expression results for the stored energy of the original lattice (i.e. not condensed and not summed):

$$E = \sum_{i=1}^{n} E_i = \sum_{i=1}^{n} \sum_{j \in B_i} \frac{1}{2} E_{ij} \tag{30}$$

where B_i is the subset ($B_i \subseteq N$) that contains all neighboring lattice nodes of lattice node i and E_{ij} is the stored energy of the truss between lattice node i and neighbor j.

For the considered lattice model, each lattice node is connected to eight neighboring nodes. Applying the summation rule of Beex et al. (2011) directly, implies that if one interaction crosses a triangle edge, the lattice node connected to that interaction will be taken into account discretely together with all the interactions connected to that lattice node. This means that seven lattice interactions will be incorporated discretely of which it is known that they have the same stored energy as other lattice interactions that are entirely located within the triangle. Therefore, the summation rule of Beex et al. (2011) is applied to the lattice trusses instead of the lattice nodes and it distinguishes the different type of lattice trusses (the horizontal, vertical and two diagonal trusses). This means that in each triangle each type of lattice truss is summed separately, i.e. in each triangle four types of internal sampling trusses may exist, each with a separate weight factor w_i. In Table 2, a possible algorithm for this fully nonlocal summation rule is given. In the subsequent section the efficiencies of previous exact summation rule and the interaction-based exact summation rule are compared.

In the following section lattice trusses that represent conductive wire segments are only present in fully resolved domains. This means that they are always incorporated discretely, i.e. they only represent themselves ($w_i = 1$). Therefore, they are not summed and therefore not shown in Table 2.

4. Results

In this section the described QC framework and lattice model are employed to study the failure surface of a patch of electronic textile that includes four conductive wires and one electronic component. The patch is subjected to different in-plane deformations, by fully prescribing all displacements of the nodes at the boundaries. Failure of the electronic textile is assumed to occur when one of the conductive wires fails. The conductive wires are assumed to fail at an engineering strain of 17%, since this is the observed engineering strain at which they fail in tensile experiments (see Fig. 3).

4.1. Reference case

The dimensions of the rectangular patch of electronic textile are 51.3 mm (178 weft yarn spacings) by 42.8 mm (266 warp yarn spacings) in horizontal and vertical direction, respectively. In Fig. 5 the used triangulation can be seen, as well as the sampling trusses for the proposed interaction-based exact summation rule.

Table 2: Selection process of sampling trusses and corresponding weight factors (w_i) for 2D computations.

▷ *for every triangle t*
- identify all lattice trusses in a rectangle circumscribing triangle t
- evaluate interpolation functions at the locations of both lattice nodes of each lattice truss
- use interpolation function evaluations to decide which lattice trusses are entirely or partially in triangle t
- produce four separate weight factors $w_i = 0$ for the four types of lattice trusses (horizontal, vertical and two diagonal trusses) that will be selected as internal sampling trusses in triangle t

▷ *for every lattice truss i belonging triangle t*

▷ *if only one lattice node of lattice truss i is located in triangle t*

- select lattice truss i as a sampling truss with $w_i = \frac{1}{2}$

▷ *else*

- determine which of the four truss types lattice truss i is

▷ *if no internal sampling truss of this type is selected yet*

- select lattice truss i as internal sampling truss of this type

▷

▷ *if lattice truss i is on an edge of triangle t*

- add $\frac{1}{2}$ to the weight factor w_i of this type

▷ *else*

- add 1 to the weight factor w_i of this type

▷

▷

▷

▷

▷ *for each sampling truss i*
- search for duplicates among the sampling trusses

▷ *for each duplicate j of sampling truss i*

- $w_i = w_i + w_j$
- remove duplicate j as sampling truss

▷

▷

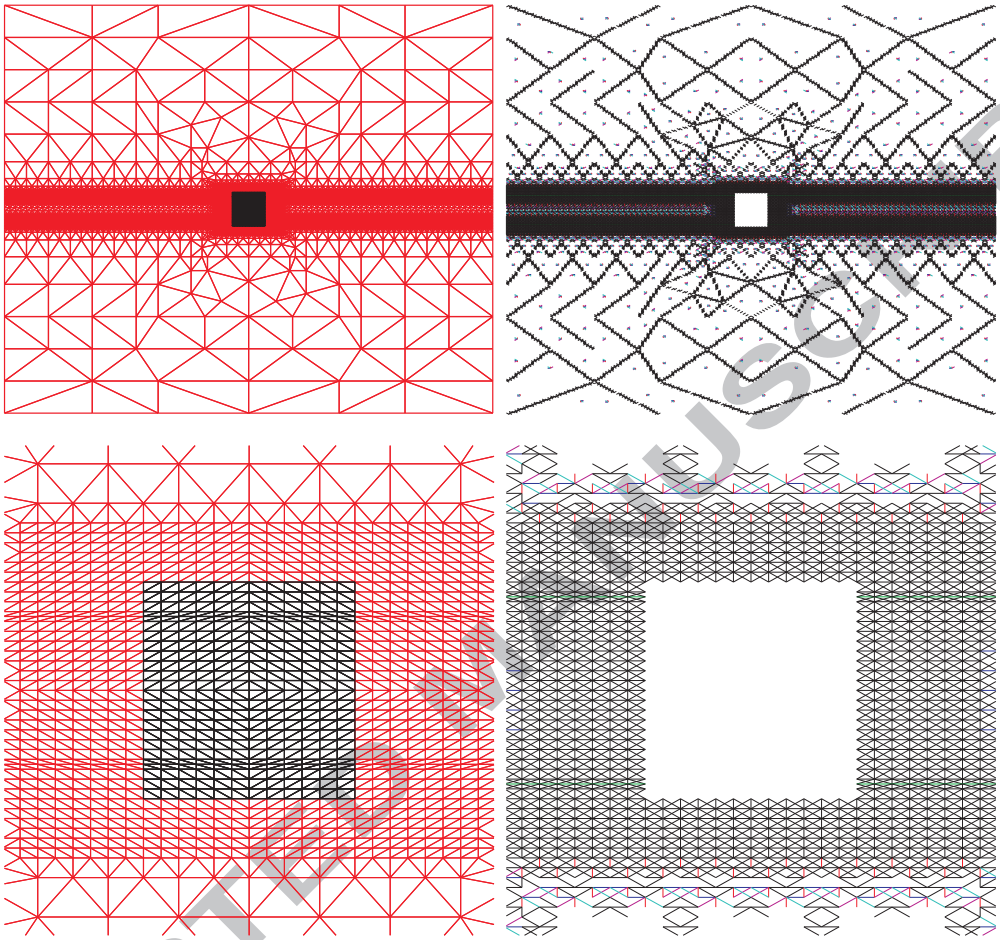

Figure 5: Top-left: the entire triangulation with the region in which stiff lattice trusses are used in black. Bottom-left: a zoom of the triangulation around the region with stiff lattice trusses. Top-right: the sampling trusses used for the QC computation. Discrete sampling trusses ($w_i = 1$) are shown in black and those that represent conductive yarn segments in green. The stiff discrete sampling trusses are not shown. Central sampling trusses ($w_i > 1$) are shown in dark blue (horizontal central sampling trusses), red (vertical central sampling trusses), magenta (diagonal central sampling trusses of the first type) and light blue (diagonal central sampling trusses of the second type). Bottom-right: the sampling trusses around the stiff discrete sampling trusses.

In the center of the model the presence of an electronic component is simulated by using different material parameters for the lattice trusses in a centered region with a size of 3.5 mm (12 weft yarn spacings) by 3.5 mm

(22 warp yarn spacings) in horizontal and vertical direction, respectively. The parameters of the lattice trusses representing the fabric are given in Table 1. All lattice trusses that represent the electronic component are given a Young's modulus of 100 GPa (independent of their orientation). This Young's modulus is used in tension as well as in compression and they only deform elastically. The dimensions of these trusses are the same as those of the other trusses. Hence, the tensile responses of the trusses representing the electronic component are at least ten times stiffer than those representing the fabric. In compression this difference is even larger (see Table 1).

Four conductive wires are connected to the electronic component (two to each side). Note that the lattice trusses that represent the conductive wires are located in the fully resolved domain. Hence, they are all selected as discrete sampling trusses ($w_i = 1$). Their material parameters are also given in Table 1. As mentioned before, the conductive wires are assumed to be located exactly between two warp yarns (see again Fig. 5) and the diagonal lattice trusses connected to them are given the same parameters as the other diagonal lattice trusses.

The QC models are loaded by prescribing all displacements of the nodes at all boundaries. Different macroscale deformations are applied in separate QC computations. These deformation are all combinations of (i) tensile deformation up to an engineering strain of 17% and (ii) simple shear up to a shear strain of 100%. The computations are subdivided into 10,000 increments, but stopped when the conductive wires fail (i.e. when the strain in one of the trusses representing the conductive wire reaches 17%).

4.1.1. Efficiency

The computational gain of the QC computation compared to the direct lattice computation can be expressed in terms of the number of DOFs (a measure for the size of the system to solve) and the relative number of sampling trusses (a measure for the effort to construct the system). We make a clear distinction here between two cases, since a smaller number of DOFs does not mean that the governing equations of QC systems are solved faster than the system of the direct lattice computation (as often assumed). This is caused by more poorly conditioned stiffness matrices rendered by QC approaches, compared to those of direct lattice computations, and the fact that iterative solvers need more time to solve poorly conditioned systems. In combination with summation rules however, the computational gain of QC approaches scales rather well with the ratio of sampling trusses, as reported by Beex et al. (2014b).

QC computations originate from atomistic lattice computations in which each interaction (here a lattice truss) is usually visited twice according to Eq. (30). In Table 3 the absolute number of lattice trusses that has to be visited to construct the governing equations is shown for (DLCa) the direct lattice computation in case each lattice truss is visited twice, (DLC) for the direct lattice computation in case each lattice truss is visited once, (ESR) for the QC approach using the exact summation rule of Beex et al. (2011) and (IESR) for the QC framework using the interaction-based modification of the exact summation rule.

Table 3: Number of DOFs and visited lattice trusses for the direct lattice computation in which each lattice truss is visited twice according to atomistic lattice computation (DLCa), the direct lattice computation in which each lattice truss is visited once (DLC), the QC computation using the exact summation rule of Beex et al. (2011) (ESR) and the interaction-based exact summation rule proposed in this study (IESR).

	DLCa	DLC	ESR	IESR
# DOFs	96,302	96,302	10,646	10,646
# lattice trusses	382,524	191,262	180,316	39,751

The numbers in Table 3 show that the interaction-based exact summation rule clearly outperforms the one of Beex et al. (2011), since the efforts to construct the governing equations (i.e. the number of visited lattice trusses) is reduced by a factor of 4.5. A gain factor of 9.6 results in comparison to the direct lattice computation in which each lattice interaction is visited twice (method DLCa in Table 3) and a factor of 4.8 compared to the direct lattice computation in which each lattice interaction is visited once (method DLC in Table 3). Hence, for the used triangulation, the previous exact summation rule (Beex et al., 2011) would hardly lead to any computational gain if the direct lattice computation is implemented such that each lattice interaction is visited once.

4.1.2. Failure surface

A typical result of the QC computation for tensile deformation is presented in Fig. 6. This figure shows the total strains of the four types of sampling trusses for the deformation at which all four conductive wires reach a strain of 17%. The largest tensile strains in the warp yarns occurs at the

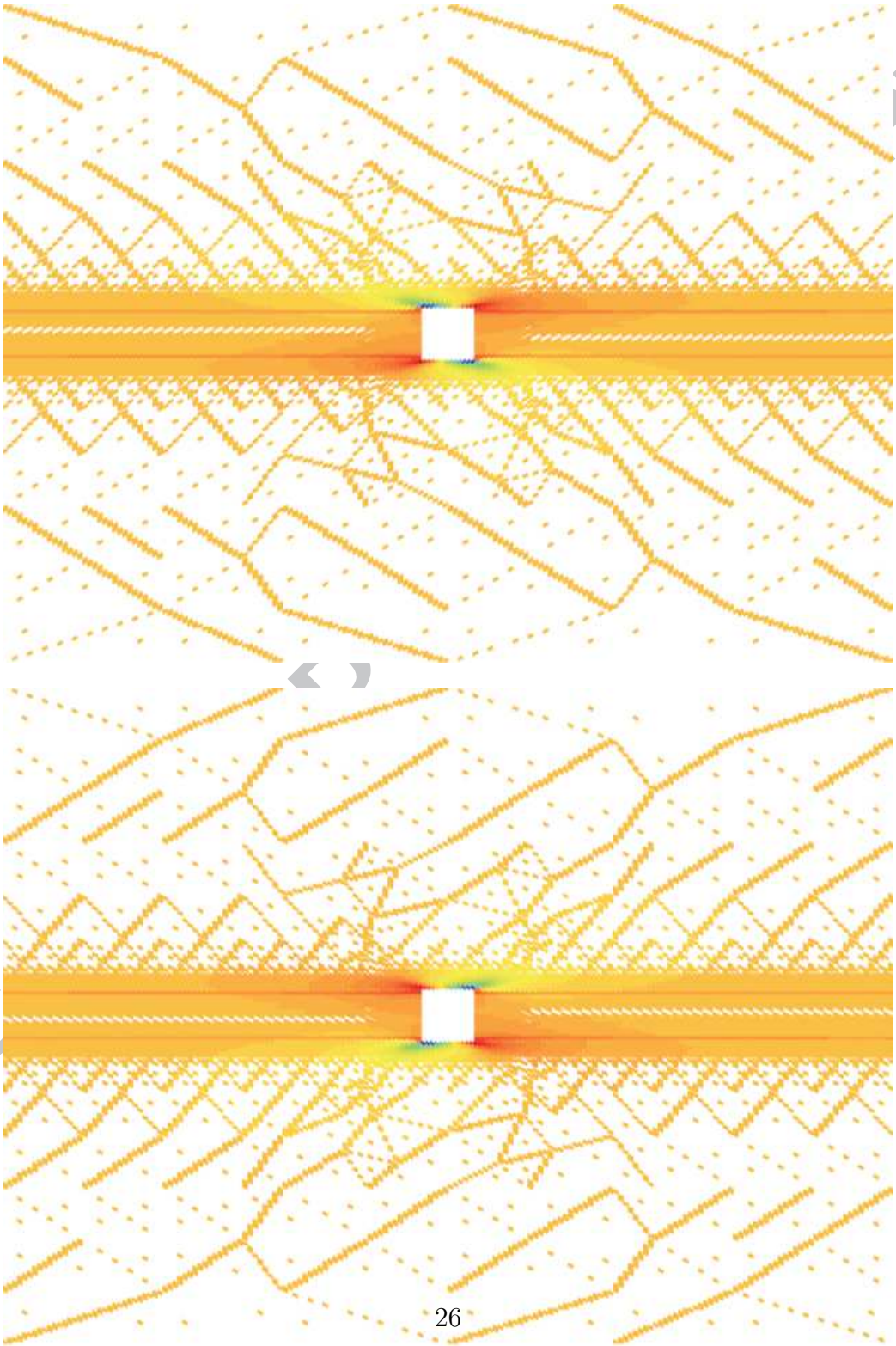

Figure 6: The engineering strains in the horizontal sampling trusses representing warp yarns (first image), the vertical sampling trusses representing weft yarns (second image), the diagonal sampling trusses oriented from bottom-left to top-right (third image) and the diagonal sampling trusses oriented from top-left to bottom-right at the tensile deformation at which the conductive wires reach 17% strain.

left-hand and right-hand side of the components, whereas the smallest tensile strains in the warp yarns are predicted to be just above and below the component. No compression of warp yarns is predicted. The predicted weft yarn strains are approximately zero, except near the four corners of the component from where the non-zero weft yarn strains decay to zero in horizontal direction. The most significant shear deformation can be observed in regions just above and below the component.

In Fig. 7, the deformation of the conductive wires is presented at the moment they fail. Rotation of the conductive wires near the electronic component is predicted as the strains of the conductive wires reaches its maximum value near the component. This shows that a simple rule of mixture is not appropriate for estimating the macroscopic horizontal strain of the electronic textile at which failure of the conductive wires occurs.

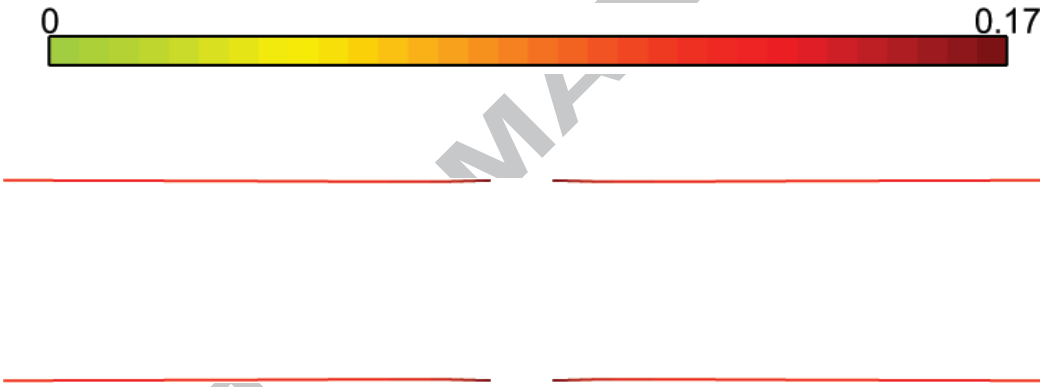

Figure 7: The engineering strains in the horizontal sampling trusses representing conductive wires at the tensile deformation at which the conductive wires reach 17% strain. The vertical direction is upscaled with a factor of 4.7.

Another typical result is presented in Fig. 8 for a tensile-shear proportional loading case 1% : 3.08%, i.e. 1% tensile elongation for 3.08% simple shear, monotonically increasing. The strains of the sampling trusses are again shown for the deformation at which one or more of the conductive wires (two in this case) reaches a total strain of 17%. The largest strains in the warp yarns be seen at the left-hand side and right-hand side near two corners of the component. From these locations the strains rapidly to zero. Above and below the same two corners, the maximum strains in the weft yarns are predicted. Significant shear deformation is present throughout the entire

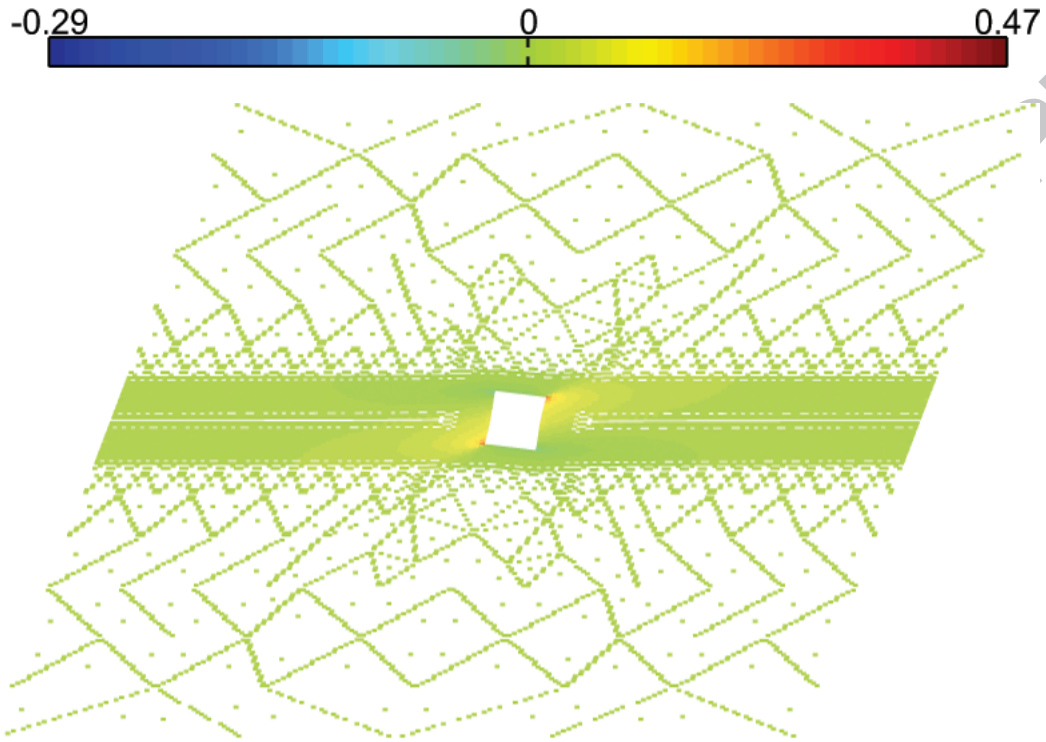

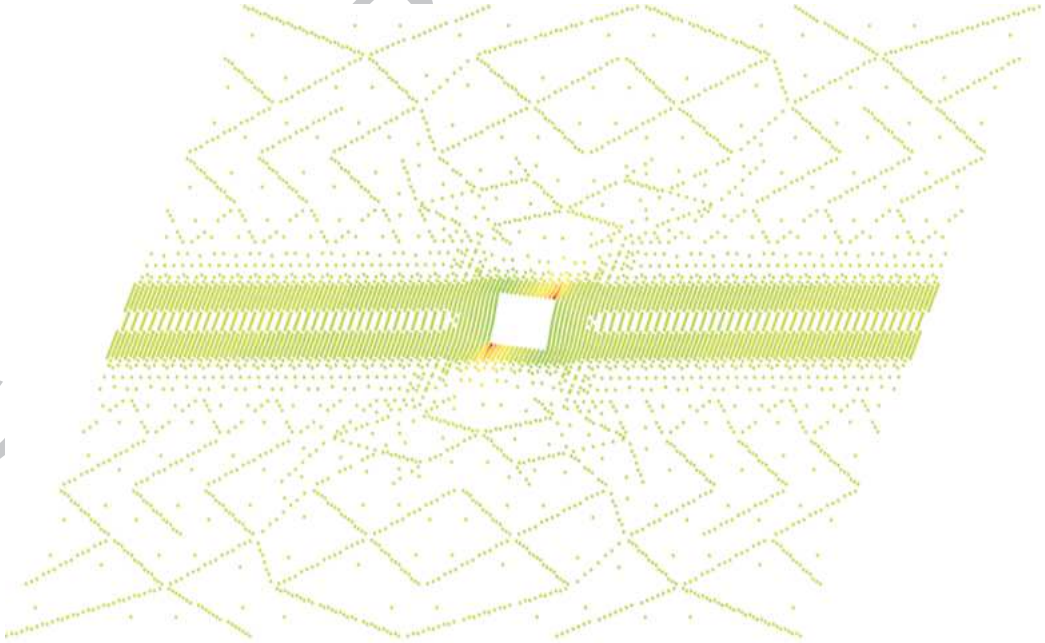

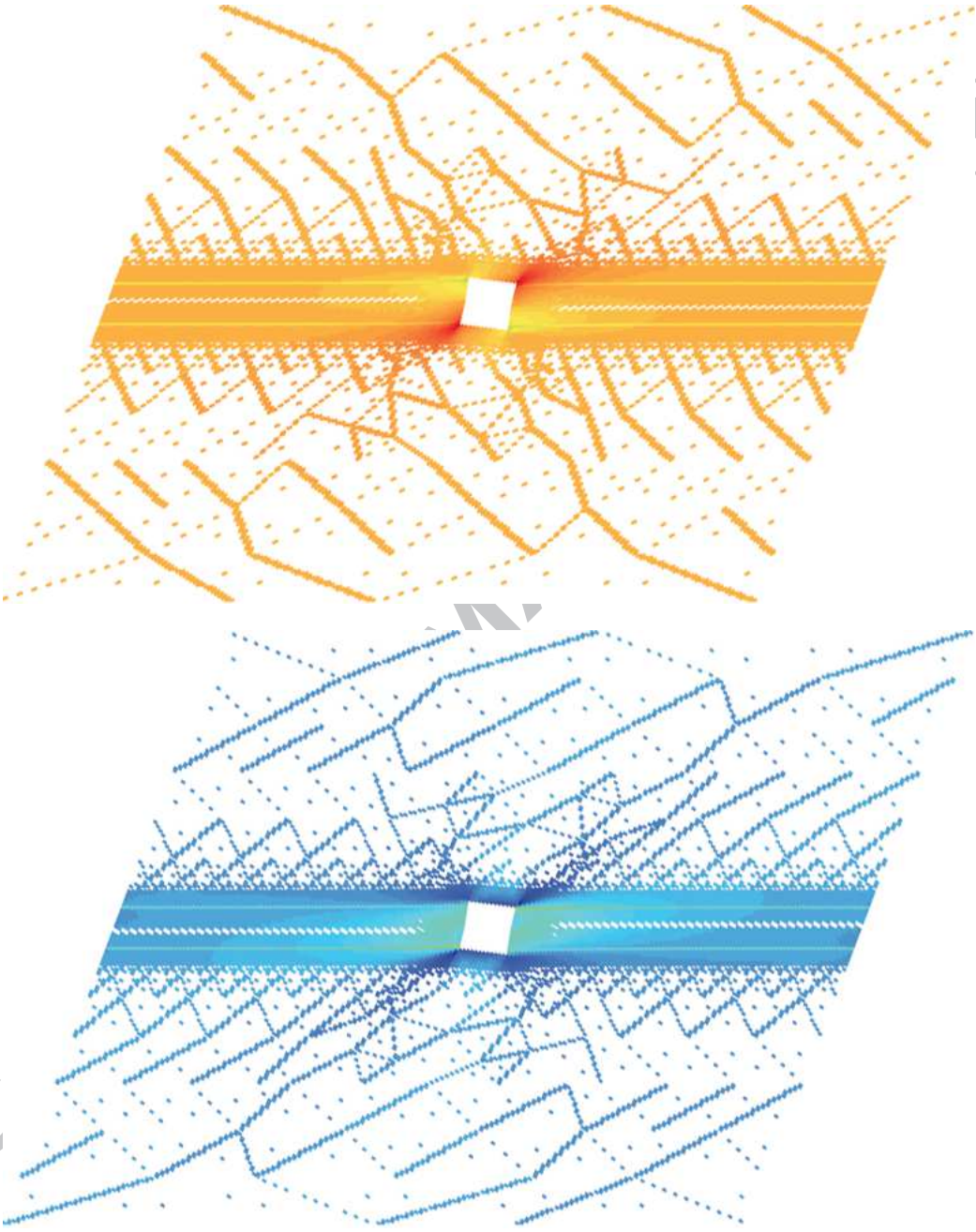

Figure 8: The engineering strains in the horizontal sampling trusses representing warp yarns (first image), the vertical sampling trusses representing weft yarns (second image), the diagonal sampling trusses oriented from bottom-left to top-right (third image) and the diagonal sampling trusses oriented from top-left to bottom-right at a combination of tensile deformation and shear deformation with a ratio of 1% : 3.08% at which the conductive wires reach 17% strain.

domain, but again the maximum values are present near the same two corners. Significant shear deformation are on the other hand also present near the other two corners of the component.

The conductive wires substantially rotate near the electronic component, compared to the uniform case. The bottom-left and top-right conductive wires fail for this macroscopic deformation, whilst the top-left and bottom-right conductive wires show only small total strains near the electronic component. This is caused by the combination of stretch in the domain far away from the electronic component and rotation near the electronic component.

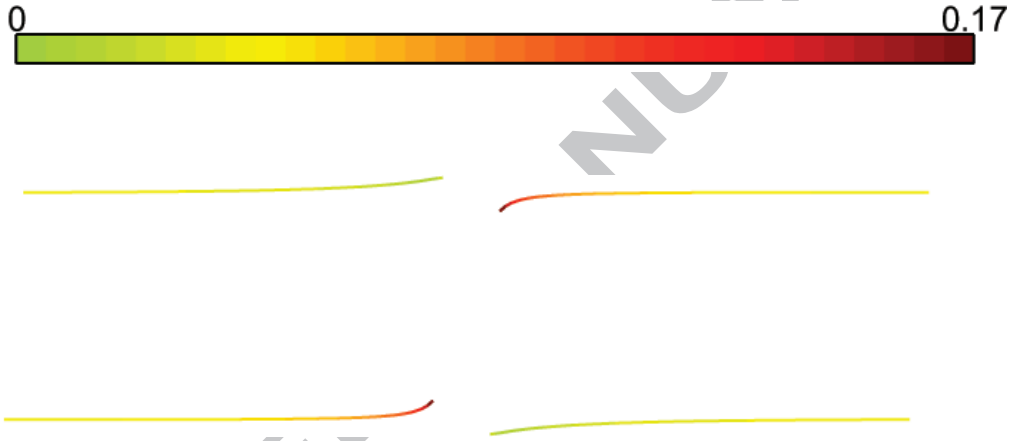

Figure 9: The engineering strains in the horizontal sampling trusses representing conductive wires at a combination of tensile deformation and shear deformation with a ratio of 1% : 3.08% at which the conductive wires reach 17%. The vertical direction is upscaled with a factor of 5.7.

Prescribing a number of different proportional ratios for extension and shear, and identifying at which deformation failure of one or more conductive wires occurs, allows to determine a failure surface. The failure surface for the reference case is shown in Fig. 10. The results shown in Fig. 6 for tensile deformation correspond with the intersection of the horizontal axis. The results shown in Fig. 8 correspond to the top point in the diagram of Fig. 10.

The failure surface in Fig. 10 shows at which macroscopic strains failure of the conductive wires occurs according to the QC computations. The failure surface reveals that more shear deformation can be applied than tensile deformation and that this particular electronic textile fails at significantly

smaller macroscopic strains than regular (non-electronic) textiles. The latter observation is undesirable for electronic textile products since they should fail at similar macroscopic strains as the plain textile to ensure that the electronic textile resembles regular textiles as much as possible. In the following subsections, different parameters are varied to investigate their influence on the macroscopic failure surface.

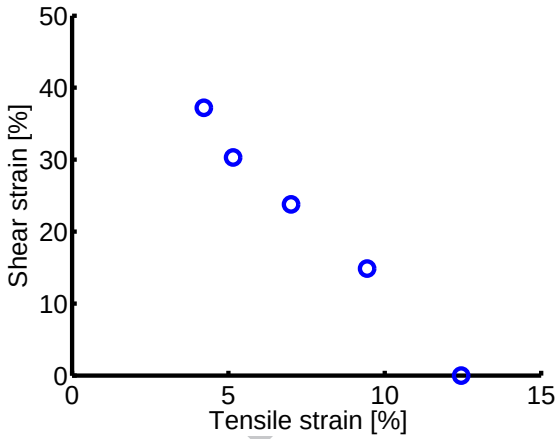

Figure 10: Failure surface of the reference case: the blue circles indicate failure of one or more conductive wires under proportional strain paths.

4.2. Influence of the location of the conductive wires

Based on the results of the reference case, it is obvious that rotation of the conductive wires occurs near the electronic components. This rotation is more pronounced for loading cases in which shear deformation is included, but rotation of the conductive wires also occurs for macroscopic tensile deformation. Figs. 6 and 8 also show that because of this rotation, the conductive wires experience the largest strain near the electronic component. Hence, failure of the conductive wires may may be shifted larger macroscopic strains if this rotation is limited.

Limiting the rotation of the conductive wires may be achieved by placing them more closely to the vertical center of the electronic component (and thus of the entire patch of electronic textile). This hypothesis is investigated by performing QC computations in which all conductive wires are located two

warp yarn spacings (0.321 mm) closer to the vertical center of the electronic component (i.e. four yarn spacings closer together).

The macroscopic failure strains at which the conductive wires fail for this configuration are shown in Fig. 11, together with the reference failure surface. The failure surface has indeed shifted towards larger macroscopic failure strains. This shows that the placement of the conductive wires indeed has a significant influence on the extensibility of the electronic textile for the case investigated here.

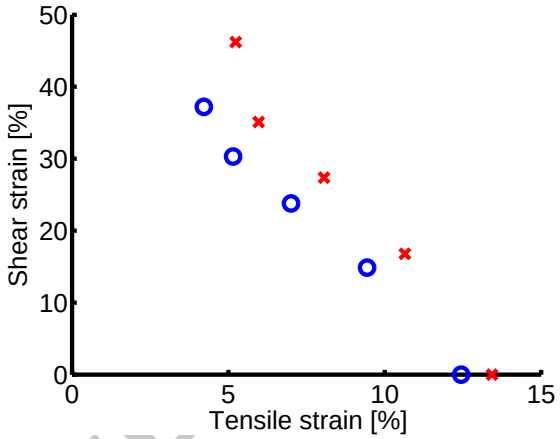

Figure 11: Failure surface in case each conductive wire is 0.322 mm (2 vertical lattice spacings) closer located to the vertical center of the electronic texile (red crosses). The blue circles indicate the failure surface of the reference case.

4.3. Influence of the diagonal response

Another interesting aspect is the influence of the textile's shear response on the failure surface. The shear response, which is governed by the diagonal trusses, (purple curve in Fig. 3) is stiff compared to other woven fabrics (Sharma et al., 2003; Sharma & Sutcliffe, 2004; Boisse et al., 2006; Lomov et al., 2008), although still very compliant compared to the warp and weft responses. If the response of the electronic textile is to resemble those of regular woven textiles, the diagonal response thus to be softer. The influence of this is investigated by performing the same set of QC computations, but with a diagonal response that is approximately twice as compliant compared

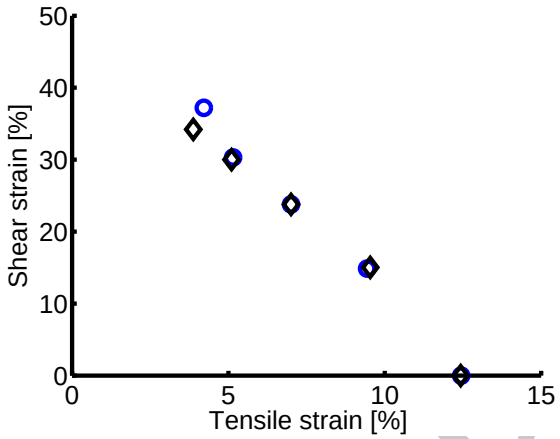

Figure 12: Failure surface in case the diagonal response is twice as compliant as in the reference (black diamonds). The blue circles indicate the failure surface of the reference case.

to the reference case. This is performed by reducing parameter H in Table 1 of the diagonal response by a factor of two.

The macroscopic failure surface for the compliant diagonal response is shown by the black diamonds in Fig. 12, together with the reference failure surface. The limited sensitivity to the shear stiffness seems convenient for the electronic textile, as the textile in the reference case has a rather stiff diagonal response compared to regular woven fabrics. These results indicate that if the diagonal response is altered such that the mechanical behaviour of the electronic textile resembles more the behaviour of other woven textiles, the failure surface will not change significantly. Changing the diagonal response of the fabric can be performed by changing the settings of the weaving process or by altering the surface roughness of the yarns, since the surface roughness has a substantial influence on the friction between the yarns that occurs during yarn rotations and hence, significantly influence the diagonal response (Grosberg and Park, 1966).

4.4. Influence of the weft response

A final textile characteristic of interest is the difference between the stiffnesses of the warp and weft yarns. As can be seen in Fig. 3, the initial stiffnesses of the trusses representing the warp yarn segments and weft yarn

segments is of the same order of magnitude. A similar set of QC computations is performed with a smaller stiffness for the weft yarns. This is done by decreasing parameter H in Table 1 of the trusses representing the weft yarn segments by a factor of two. This effectively lowers the stiffness of these trusses by a factor of 1.8.

Reconstructing the failure surface under proportional loading paths gives Fig 13. The effect is again insignificant compared to the effect of locating the conductive wires closer to the vertical center of the electronic component.

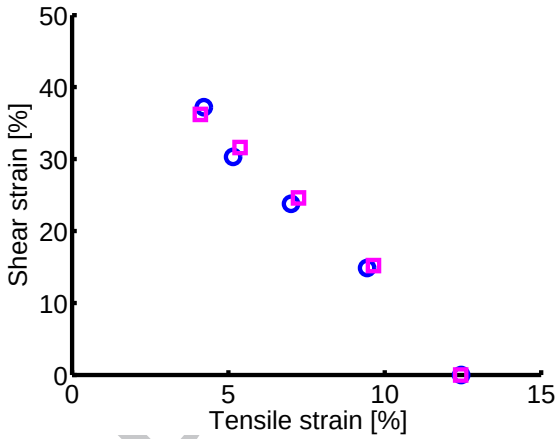

Figure 13: Failure surface in case the weft (vertical direction) response is twice as compliant as in the reference (purple squares). The blue circles indicate the failure surface of the reference case.

5. Conclusion

The three main novelties presented in this paper are that:

- the virtual-power-based QC method is used to investigate the mechanical behaviour of a true material,
- the influence of geometric and material parameters on the mechanical reliability of an electronic textile with an embedded component is investigated, and
- interaction-based summation, in contrast to node-based summation, is used to reduce the efforts to construct the governing equations.

The macroscopic failure surface of an electronic textile is determined on the basis of a dissipative lattice model, previously proposed for electronic textile (Beex et al., 2013a). A virtual-power-based quasicontinuum (QC) method (Beex et al., 2014b) is used to reduce the computational costs of the direct lattice computations. As the lattice model includes dissipation, a virtual-power-based QC method, developed for non-conservative lattices is required, as all previous QC methodologies can only be used for conservative lattices which are in practise almost solely used for atomistic lattices (Tadmor et al., 1996a,b; Knap & Ortiz, 2001; Miller & Tadmor, 2002; Marian et al., 2008; Eidel & Stukowski, 2009).

The summation rule used in the present QC methodology is an interaction-based variant of the exact summation rule of (Beex et al., 2011), which determines the governing equations of the condensed/interpolated lattice exactly. The interaction-based summation proposed in this contribution preserves exactness and hence, it only influences bookkeeping. The modification consist of summing over the sampling interactions directly, instead of summing over sampling nodes which are then used to sum over sampling interactions. The latter summation principle originates from atomistic lattice modelling, but is not required for lattices that are governed by local, nearest neighbour interactions as considered in structural lattices. The influence of the interaction-based summation for the computation costs is significant as shown in this contribution; an additional computational gain of a factor of 4.5 is observed for the triangulation used. In the considered triangulation, the difference between the fully resolved region and the coarse domain is rather limited. This means that even larger additional computational gains can be achieved if the difference between the fully resolved region and the coarse region are larger, which are very likely to be present in engineering scale applications.

The computations are performed on a patch of electronic textile with one embedded rectangular electronic component that is connected at its left and right edges to two conductive wires that are woven in the fabric. In the computations different proportional tensile-shear loading paths have been prescribed. The failure surface is determined by identifying at which macroscopic deformation one or more of the conductive wires reach a strain of 17%; i.e. the strain at which the conductive wires fails.

The results have shown that placing the conductive wires closer towards the vertical center of the electronic component leads to larger failure strains. Since the diagonal response of the investigated electronic textile was stiff compared to those of other woven fabrics and the mechanical behaviour of

the electronic textile should resemble a regular textile as closely as possible, the influence of reducing the diagonal response was investigated as well. The results have shown that reducing the effective stiffness of the diagonal response by a factor of two hardly influences the failure surface.

Acknowledgements

The authors gratefully acknowledge Steven Luitjens of Royal Philips Electronics N.V. for his input in many discussions on electronic textile. Furthermore, they thank Edward de Boer for his precise experimental work on individual conductive wires. This research is supported by the Dutch Technology Foundation STW, which is the applied science division of NWO, and the Technology Programme of the Ministry of Economic Affairs under Project Nr. 10104.

References

Bonderover, E., Wagner, S., 2004, A woven inverter circuit for e-textile applications, IEEE Electronic Device Letters 25, 295-297.

Beex, L.A.A., Peerlings, R.H.J., Geers, M.G.D., 2011, A quasicontinuum methodology for multiscale analyses of discrete microstructures, International Journal for Numerical Methods in Engineering 87, 701-718.

Beex, L.A.A., Verberne, C.W., Peerlings, R.H.J., 2013a, Experimental identification of a lattice model for woven fabrics: application to electronic textile, Composites Part A 48, 82-92.

Beex, L.A.A., Peerlings, R.H.J., Geers, M.G.D., 2013c, Central summation in the quasicontinuum method, Submitted.

Beex, L.A.A., Peerlings, R.H.J., Geers, M.G.D., 2014a, A multiscale quasicontinuum framework for lattice models with bond failure and fiber sliding, Computer Methods in Applied Mechanics and Engineering 269, 108-122.

Beex, L.A.A., Peerlings, R.H.J., Geers, M.G.D., 2014b, A multiscale quasicontinuum method for dissipative lattice models and discrete networks, Journal of the Mechanics and Physics of Solids 64, 154-169.

Ben Boubaker, B., Haussy, B., Ganghoffer, J.F., 2007a, Discrete models of woven structures. Macroscopic approach, Composites Part B 38, 498-505.

Ben Boubaker, B., Haussy, B., Ganghoffer, J.F., 2007b, Considerations of the yarn-yarn interactions in meso/macro discrete model of fabric Part II: Woven fabric under uniaxial and biaxial extension, Mechanics Research Communications 34, 371-378.

Boisse, P., Gasser, A., Hivet, G., 2001, Analyses of fabric tensile behaviour: determination of the biaxial tension-strain surfaces and their use in forming simulations, Composites Part A 32, 1395-1414.

Boisse, P., Zouari, B., Daniel, J.L., 2006, Importance of in-plane shear rigidity in finite element analyses of woven fabric composite preforming, Composites Part A 37, 2201-2212.

Coosemans, J., Hermans, B., Puers, R., 2006, Integrating wireless ECG monitoring in textiles, Sensors and Actuators A: Physical 130-131, 48-53.

Dalton, A.B., Colins, S., Muñz E, Razal, J.M., Von Howard, E., Ferraris, J.P., Coleman, J.N., Kim, B.G., Baughman, R.H., 2003, Super-tough carbon-nanotube fibres, Nature 423, 703.

De Rossi, D., 2007, Electronic textiles: a logical step, Nature Materials 6, 328-329.

Edmison, J., Jones, M., Nakad, Z., Martin, T., 2002, Using piezoelectric materials for wearable electronic textiles, Proceedings of the 6th International Symposium on Wearable Computers, 41-48.

Eidel, B., Stukowski, A., 2009, A variational form of the quasicontinuum method based on energy sampling in clusters, Journal of the Mechanics and Physics of Solids 57, 87-108.

Germain, P., 1973, The method of virtual power in continuum mechanics Part 2: microstructure, SIAM Journal on Applied Mathematics 25, 556-575.

Grosber, P., Park, B.J. 1966, The Mechanical Properties of Woven Fabrics Part V: The Initial Modulus and the Frictional Restraint in shearing of Plain Weave Fabrics, Textile Research Journal 36, 420-431.

King, M.J., Jearanaisilawong, P., Socrate, S., 2005, A continuum constitutive model for the mechanical behavior of woven fabrics, International Journal of Solids and Structures 42, 3867-3896.

Knap, J., Ortiz, M., 2001, An analysis of the quasicontinuum method, Journal of the Mechanics and Physics of Solids 49, 1899-1923.

Kulachenko, A., Uesaka, T., 2012, Direct simulation of fiber network deformation and failure, Mechanics of Materials 51, 1-14.

Lomov, S.V., Verpoest, I., 2006, Model of shear of woven fabrics and parametric description of shear resistance of glass woven reinforcements, Composites Science and Technology 66, 919-933.

Lomov, S.V., Ivanov, D.S., Verpoest, S., Zako, M., Kurashiki, T., Nakai, H., Hirosawa, S., 2007, Meso-FE modelling of textile composites: Road map, data flow and algorithms, Composite Science and Technology 67, 1870-1891.

Lomov, S.V., Boisse, P., Deluycker, E., Morestin, F., Vanclooster, K., Vandepitte, D., Verpoest, I., Willems, A., 2008, Full-field strain measurement in textile deformability studies, Composites Part A 39, 1232-1244.

Marian, J., Knap, J., Campbell, G.H., 2008, A quasicontinuum study of nanovoid collapse under uniaxial loading in Ta, Acta Materiala 56, 2389-2399.

Marlescu, D., Marlescu, R., Zamora, N.H., Stanley-Marbell, P., Khosla, P.K., Park, S., Jayaraman, S., Jung, S., Lauterbach, C., Weber, W., Kirstein, T., Cottet, D., Grzyb, J., Tröster, G., Jones, M., Martin, T., Nakad, Z., 2003, Electronic textiles: a platform for pervasive computing, Proceedings of the IEEE 91, 1995-2018.

Miller, R.E., Tadmor, E.B., 2002, The quasicontinuum method: overview, applications and current directions, Journal of Computer-Aided Materials Design 9, 203-239.

Nakad, Z., Jones M., Martin, T., Shenoy, R., 2007, Using electronic textiles to implement an acoustic beamforming array: a case study, Pervasive and Mobile Computing 3, 581-606.

Nilakantan, G., Keefe, M., Bogetti, T.A., Adkinson, R., Gillespie, J.W.Jr., 2010, On the finite element analysis of woven fabric impact using multiscale modelling techniques, International Journal of Solids and Structures 47, 2300-2315.

Peng, X.Q., Cao, J., 2005, A continuum mechanics-based non-orthogonal constitutive model for woven composite fabrics, Composites Part A 36, 859-874.

Potluri, P., Manan, A., 2007, Mechanics of non-orthogonally interlaced textile composites, Composites Part A 38, 1216-1226.

Potluri, P., Sagar, T.V., 2008, Compaction modelling of textile preforms for composite structures, Composite Structures 86, 177-185.

Ridruejo, A., González, C., Llorca, J, 2010, Damage micromechanisms and notch sensitivity of glass-fiber non-woven felts: an experimental and numerical study, Journal of the Mechanics and Physics of Solids 58, 1628-1645.

Sharma, S.B., Sutcliffe, M.P.F., Chang, S.H., 2003, Characterization of material properties for draping of dry woven composite material, Composites Part A 34, 1167-1175.

Sharma, S.B., Sutcliffe, M.P.F., 2004, A simplified finite element model for draping of woven material, Composites Part A 35, 637-643.

Shenoy, V.B., Miller, R., Tadmor, E.B., Rodney, D., Phillips, R., Ortiz, M., 1999, An adaptive finite element approach to atomistic scale mechanics - the quasicontinuum method, Journal of the Mechanics and Physics of Solids, Vol. 47, 611-642.

Tadmor, E.B., Phillips, R., Ortiz, M., 1996a, Mixed atomistics and continuum models of deformation in solids, Langmuir 12, 4529-4534.

Tadmor, E.B., Ortiz, M., Phillips, R., 1996b, Quasicontinuum analysis of defects in solids, Philosophical Magazine A 73, 1529-1563.

Ten Thije, R.H.W., Akkerman, R., Húetink, J., 2007, Large deformation simulation of anisotropic material using an updated Lagrangian finite element method, Computer Methods in Applied Mechanics and Engineering 196, 3141-3150.

Ten Thije, R.H.W., Akkerman, R., 2008, Solutions to intra-ply shear locking in finite element analyses of fibre reinforced materials, Composites Part A 39, 1167-1176.

Wang, X., Guo, X., Su, Z., 2014, A quasi-continuum model for human erythrocyte membrane based on the higher-order Cauchy-Born rule, Computer Methods in Applied Mechanics and Engineering 268, 284-298.

Wilbrink, D.V., Beex, L.A.A., Peerlings, R.H.J., 2013, A discrete network model for bond failure and frictional sliding in fibrous materials, International Journal of Solids and Structures 50, 1354-1363.

Zhu, B., Yu, T.X., Tao, X.M., 2007, Large deformation and slippage mechanism of plain woven composite in bias extension, Composites Part A 38, 1821-1828.

Zohdi, T.I., Powell, D., 2006, Multiscale construction and large-scale simulation of structural fabric undergoing ballistic impact, Computer Methods in Applied Mechanics and Engineering 195, 94-109.

Zysset, C., Kinkeldei, T., Cherenack, K., Tröster, G., 2010, Woven electronic textiles: an enabling technology for health-care monitoring in clothing, Proceedings of UbiComp 2010, 843-848.

- The virtual-power-based quasicontinuum method is used to investigate a true material
- The mechanical reliability of an electronic textile with a component is investigated
- Interaction-based summation is developed, opposed to node-based summation